UNIVERSITY
OF TRENTO

DEPARTMENT OF INFORMATION AND COMMUNICATION TECHNOLOGY

38050 Povo – Trento (Italy), Via Sommarive 14
http://www.dit.unitn.it

AN ADAPTIVE SEMI-PARAMETRIC AND CONTEXT-BASED APPROACH TO UNSUPERVISED CHANGE DETECTION IN MULTITEMPORAL REMOTE-SENSING IMAGES

Lorenzo Bruzzone and Diego Fernández Prieto

2002

Technical Report # DIT-02-0030

Also: appeared on IEEE Transactions on Image Processing, Vol. 11, No. 4, 2002

An Adaptive Semi-Parametric and Context-Based Approach to Unsupervised Change Detection in Multitemporal Remote-Sensing Images

Lorenzo Bruzzone, *Member, IEEE,* and Diego Fernàndez Prieto, *Student Member, IEEE*

DIT - University of Trento, Via Sommarive, 14, 38050, Trento, Italy

e-mail: lorenzo.bruzzone@ing.unitn.it

***Abstract* – In this paper, a novel automatic approach to the unsupervised identification of changes in multitemporal remote-sensing images is proposed. This approach, unlike classical ones, is based on the formulation of the unsupervised change-detection problem in terms of the Bayesian decision theory. In this context, an adaptive semi-parametric technique for the unsupervised estimation of the statistical terms associated with the gray levels of changed and unchanged pixels in a difference image is presented. Such a technique exploits the effectivenesses of two theoretically well-founded estimation procedures: the reduced Parzen estimate (RPE) procedure and the expectation-maximization (EM) algorithm. Then, thanks to the resulting estimates and to a Markov Random Field (MRF) approach used to model the spatial-contextual information contained in the multitemporal images considered, a change detection map is generated. The adaptive semi-parametric nature of the proposed technique allows its application to different kinds of remote-sensing images. Experimental results, obtained on two sets of multitemporal remote-sensing images acquired by two different sensors, confirm the validity of the proposed approach.**

Index terms* - *Change detection, multitemporal images, remote sensing, adaptive semi-parametric estimation, Bayes theory, reduced Parzen estimate, expectation-maximization algorithm.

I. INTRODUCTION

Automatic change detection in images of a given scene acquired at different times is one of the most interesting topics of image processing. It finds important applications within different contexts, ranging from video surveillance [1], [2] to video coding [3], [4], tracking of moving objects [5], [6], and motion estimation [7], [8]. Recently, the increasing interest in the field of environmental protection has led to the recognition of the fundamental role played by change-detection techniques in monitoring the earth's surface [1], [9]-[14]. In this respect, the importance of change-detection methods relies on the possibility of identifying changes that occurred in land covers (e.g. due to urban expansion, deforestation, floods, forest fires, etc.) by analyzing multispectral images acquired at different dates by use of sensors mounted on board of satellites.

Change detection in multitemporal remote-sensing images is characterized by several peculiar factors that render ineffective some of the multitemporal image analysis techniques typically used in other application domains. The main difficulties affecting change detection in remote-sensing images arise from [10], [11], [13]: the lack of a-priori information about the shapes of changed areas; the absence of a reference background; differences in light conditions, atmospheric conditions, sensor calibration, and ground moisture at the two acquisition dates considered; problems of alignment of multitemporal images (registration noise). These factors restrict the use of most classical multitemporal image-analysis techniques to few particular remote-sensing problems; for instance, model-based approaches can be adopted only for special purposes, like detection of specific man-made objects [1].

In the literature, several supervised and unsupervised techniques for detecting changes in remote-sensing images have been proposed [1], [9]-[16]. The former require the availability of a "ground truth" from which to derive a training set containing information about the spectral signatures of the changes that occurred in the considered area between the two dates. The latter performs change detection without any additional information besides the raw images considered. Therefore, from an operational point of view, it is obvious that using unsupervised techniques is mandatory in many remote-sensing applications, as suitable ground-truth information is not always available.

This paper deals with the widely used type of unsupervised techniques that perform change detection through a direct comparison of the original raw images acquired in the same area at two different times. The change-detection process performed by such unsupervised techniques is usually divided into three main sequential steps: 1) pre-processing, 2) image comparison and 3) analysis of the difference image. These steps

are detailed in the following.

1) *Preprocessing* - Unsupervised change-detection algorithms usually take two digitized images as input and return the locations where differences between the two images can be identified. To accomplish such a task, a preprocessing step is necessary aimed at rendering the two images comparable in both the spatial and spectral domains.

   Concerning the spatial domain, the two images should be co-registered so that pixels with the same coordinates in the images may be associated with the same area on the ground. This is a very critical step, which, if inaccurately performed, may render change-detection results unreliable (we refer to [10] for more details on the impact of registration noise on the accuracy of change detection, to [17]-[19] for techniques aimed at supporting the registration process, and to [11], [20] and [21] for techniques devoted to reducing registration noise).

   With regard to the spectral domain, changes in illumination and atmospheric conditions between the two acquisition times may be a potential source of errors and should be taken into account in order to obtain accurate results [22]-[23]. This problem can be mitigated by performing a radiometric calibration of the images. To this end, two different approaches can be taken: absolute calibration and relative calibration. The former involves the conversion of the grey-level values in the images into the corresponding ground reflectance values [25]-[27]. The latter aims at modifying the histograms of the images so that the same grey-level values in the two images may represent the same reflectance values, whatever the reflectance values on the ground may be [22], [23], [27]. The choice of one of the two approaches depends on the particular application considered and on the specific information available. Generally, in remote-sensing applications, illumination can be assumed to change smoothly with respect to the pixel coordinates in each image considered. Therefore, in many cases, one can divide an original scene into different *areas of interest* (AOIs), so that that differences in illumination conditions will be constant for each pixel in a given area of interest. Hence, a separate analysis of each AOI allows the suppression of the main effects of varying illumination on the change-detection process. It is worth noting that selecting the AOI dimensions should involve a tradeoff between obtaining uniform illumination conditions and relying on sufficient statistics for

carrying out the change-detection process. However, even though selecting the AOI size may be a critical issue in other application domains, usually it does not represent a serious limitation in operational remote sensing. In fact, illumination variations inside images acquired by space-borne sensors are usually smooth enough to allow operators to easily select a suitable size. The reader is referred to [7] for a more detailed analysis of this issue.

2) *Image comparison* - The two registered and corrected images (or a linear or non-linear combination of the spectral bands of such images [13]) are compared, pixel by pixel, in order to generate a further image ("difference image"). The difference image is computed in such a way that pixels associated with land-cover changes present gray-level values significantly different from those of pixels associated with unchanged areas [13]. For example, the univariate image *differencing* (UID) technique [12], [13] generates the difference image by subtracting, on a pixel basis, a single spectral band for each of the two multispectral images under analysis. The choice of the spectral band to be subtracted depends on the specific type of change to be detected. An analogous concept is followed by the widely used change vector analysis (CVA) technique. In this case, several spectral channels are considered at each date (i.e. each pixel of the image considered is represented by a vector whose components are the gray-level values associated with that pixel in the different spectral channels selected). Then, for each pair of corresponding pixels, the so-called "spectral change vector" is computed as the difference in the feature vectors at the two times. At this point, the pixels in the difference image are associated with the magnitudes of the spectral change vectors; it follows that unchanged pixels present small gray-level values, whereas changed pixels present rather large values.

3) *Analysis of the difference image* - Land-cover changes can be detected by applying a decision threshold to the histogram of the difference image. For instance, when the CVA technique is used (i.e. each pixel in the difference image is associated with the magnitude of the difference between the corresponding feature vectors in the original images), changed pixels can be identified on the right side of the histogram as they are associated with large gray-level values. The selection of the decision threshold is of major importance as the accuracy of the final change-detection map strongly depends on this choice. Although in the image processing literature some automatic techniques for choosing a suitable decision threshold for change-

detection problems have been proposed [28], in remote-sensing applications such a choice has generally been made by using non-automatic heuristic strategies based on trial-and-error approaches [11], [13], [29]. The classical approach to choosing the decision threshold implies the assumption (reasonable but not always verified) that few changes occurred between the two dates considered. Under this hypothesis, the density function of the pixel gray-level values in the difference image may be confused with the density function of the unchanged pixels. Under this assumption, a decision strategy based on the single-hypothesis testing theory can be adopted [30], i.e. pixels with gray-level values significantly different from the mean of the density function of the difference image are labeled as changed. When this strategy is used, the decision threshold is typically fixed at $n s_D$ from the mean value of the difference image, s_D being the standard deviation of the density function of the pixel gray-level values in the difference image and n a real number derived by a trial-and-error procedure. Some authors [31]-[33] have experimentally studied the effects of different n values on the accuracy of change-detection results.

In this paper, we focus on the last step of the change-detection process. In particular, we propose a novel approach to the analysis of the difference image that overcomes the aforementioned drawback, i.e. the lack of effective and theoretically founded procedures for an automatic identification of changes in a difference image. Such an approach is based on the assumption that the histogram of the difference image can be modeled as a mixture density composed of the distributions of two classes associated with changed and unchanged pixels, respectively. In this context, an adaptive semi-parametric and unsupervised method for the estimation of the conditional density functions of these classes is proposed. The present method, which is an extension to the parametric technique presented in [34], exploits the effectivenesses of two theoretically well-founded estimation procedures: the reduced Parzen estimate (RPE) procedure [35] and the expectation-maximization (EM) algorithm [36]-[38]. In particular, the RPE procedure is used to derive initial non-parametric estimates of the probability density functions of changed and unchanged pixels in the difference image. Then, these non-parametric estimates are iteratively improved by using the EM algorithm to provide a more accurate description of the difference-image statistics. We define this estimation procedure as an adaptive semi-parametric approach. On the one hand, the term "adaptive" points out the fact that the

proposed method does not assume any a-priori model on the data distribution; this allows one to apply the present approach to different kinds of remote-sensing images (e.g. optical and SAR images). On the other hand, the term "semi-parametric" refers to the nature of the final estimates, which are derived by converting the initial non-parametric model into a more suitable semi-parametric description of the difference-image statistics (these aspects will be clarified in Section III).

In addition, the proposed approach, unlike classical techniques for unsupervised change detection in remote-sensing applications [13], uses the spatial-contextual information contained in the difference image in order to increase the accuracy of the final change-detection map. In particular, a method based on Markov Random Fields (MRFs) is proposed that exploits the interpixel class dependence to model the prior probabilities of the classes. This allows both the accuracy and the reliability of the final change-detection map to be increased.

The paper is organized into six sections. The problem formulation and the general description of the proposed technique are provided in Section II. In Section III, the method for estimating the statistical terms necessary to apply the Bayesian theory is detailed. In Section IV, the data sets used for the experiments are described. Experimental results are reported in Section V. Finally, in Section VI, results are discussed and conclusions are drawn.

II. Problem Formulation and General Description of the Proposed Technique

Let us consider two co-registered multispectral images, $\mathbf{X_1}$ and $\mathbf{X_2}$, acquired by a space-borne sensor in the same geographical area at two different times, t_1 and t_2. Let $\mathbf{X_1^{AOI}} = \{X_1^{AOI}(i,j), 1 \le i \le I, 1 \le j \le J\}$ and $\mathbf{X_2^{AOI}} = \{X_2^{AOI}(i,j), 1 \le i \le I, 1 \le j \le J\}$ be two corresponding AOIs of size $I \times J$ extracted from the original images $\mathbf{X_1}$ and $\mathbf{X_2}$, respectively (Table I provides a summary of all the variables used in the paper). Let us assume that illumination variations in the selected AOI can be considered to present a constant behavior versus the pixel coordinates. Let X be a random variable that represents the values of the $I \times J$ pixels in the difference image $\mathbf{X_D} = \{X(i,j), 1 \le i \le I, 1 \le j \le J\}$; such values have been obtained by applying to $\mathbf{X_1^{AOI}}$ and $\mathbf{X_2^{AOI}}$ the CVA technique [13] (i.e. $X(i,j) = \left\| X_1^{AOI}(i,j) - X_2^{AOI}(i,j) \right\|$); the generalization of the method to

other techniques based on the difference image is straightforward.

Unlike classical unsupervised techniques used in remote-sensing applications, we formulate the change-detection problem in terms of the Bayesian decision theory. In this context, for a given pixel in the difference image $\mathbf{X_D}$, we want to choose one of two classes, w_c and w_n, associated with changed and unchanged pixels, respectively. Let the set $\mathbf{C} = \{\mathbf{C}_l, 1 \le l \le L\}$, with $L = 2^{IJ}$, be composed of all the possible sets of labels in the difference image $\mathbf{X_D}$, where $\mathbf{C}_l = \{C_l(i,j), 1 \le i \le I, 1 \le j \le J\}$, with $C_l(i,j) \in \{w_n, w_c\}$, is a generic set of labels in $\mathbf{X_D}$. Let us define the neighbor system of the pixel with the coordinates *(i,j)* as $\mathbf{N}(i,j) = \{(i,j) + (v,\varsigma), (v,\varsigma) \in \mathbf{N}\}$, where $\mathbf{N}$ is a specific spatial neighborhood system (in this paper, we shall consider a second-order spatial neighborhood system $\mathbf{N} = \{(\pm 1,0),(0,\pm 1),(1,\pm 1),(-1,\pm 1)\}$).

In terms of the Bayesian formulation, the set of labels $\mathbf{C}_k$ that minimize the overall change-detection error can be derived by using the following decision rule:

$$\mathbf{C}_k = \underset{\mathbf{C}_l \in \mathbf{C}}{arg\,max} \{P(\mathbf{C}_l / \mathbf{X}_D)\} = \underset{\mathbf{C}_l \in \mathbf{C}}{arg\,max} \{P(\mathbf{C}_l) p(\mathbf{X}_D / \mathbf{C}_l)\} \quad (1)$$

where $P(\mathbf{C}_l)$ is the prior model for the class labels, and $p(\mathbf{X}_D/\mathbf{C}_l)$ is the joint density function of the pixel values in the difference image, given the set of labels $\mathbf{C}_l$. The application of (1) requires the estimations of both $P(\mathbf{C}_l)$ and $p(\mathbf{X}_D/\mathbf{C}_l)$, which are very complex tasks. To simplify the problem, we make two widely used assumptions: 1) we model the spatial-contextual information in a local spatial neighborhood (this is rather a reasonable approach, given the interpixel class dependence, as the interactions between pixel labels decrease rapidly as the distances between pixels increase [39]); 2) we assume the following conditional independence:

$$p(\mathbf{X_D} / \mathbf{C_l}) = \prod_{X(i,j) \in \mathbf{X}_D} p[X(i,j)/C_l(i,j)]. \quad (2)$$

It is worth noting that the validity of the last assumption is difficult to demonstrate and in our application it may be more critical than in other cases. However, from the computational viewpoint, it can be considered a reasonable simplification that allows a good trade-off between theoretical aspects and computational complexity.

We can use an MRF approach to modeling the spatial context in the prior model for the class labels $P(\mathbf{C}_l)$.

According to (1), the generation of the final change-detection map involves the labeling of all the pixels

in the difference image so that, under the aforesaid assumptions, the posterior probability may be maximized. In terms of the Markovian approach, this is equivalent to minimizing the following energy function [40]-[42]:

$$U(X_D, C_l) = \sum_{i=1}^{I}\sum_{j=1}^{J}\left[U_{context}\left(C_l(i,j)/\{C_l(g,h),\ (g,h)\in \mathbf{N}(i,j)\}\right) + U_{data}\left(X(i,j)/C_l(i,j)\right)\right] \quad (3)$$

The energy term $U_{context}(\cdot)$ describes the interpixel class dependence, whereas the term $U_{data}(\cdot)$ represents the statistics of the gray levels in the difference image under the assumption of conditional independence, as defined in (2).

For the estimation of $U_{context}(\cdot)$, we suggest using the simple MRF model presented in [34], [43]. In particular, the Markov modeling of the conditional distribution of the pixel label $C_l(i,j)$, given the pixel labels elsewhere, can be expressed as [40]-[43]:

$$P\left(C_l(i,j)/\{C_l(g,h),\ (g,h)\neq(i,j)\}\right) = P\left(C_l(i,j)/\{C_l(g,h),\ (g,h)\in \mathbf{N}(i,j)\}\right) =$$

$$= \frac{1}{Z}\exp\left[-U_{context}\left(C_l(i,j)/\{C_l(g,h),\ (g,h)\in \mathbf{N}(i,j)\}\right)\right] \quad (4)$$

where $U_{context}(\cdot)$ is the Gibbs energy function and Z is a normalizing factor. $U_{context}\left(C_l(i,j)/\{C_l(g,h),\ (g,h)\in \mathbf{N}(i,j)\}\right)$ is defined as [40]-[43]:

$$U_{context}\left(C_l(i,j)/\{C_l(g,h),\ (g,h)\in \mathbf{N}(i,j)\}\right) = \sum_{(g,h)\in \mathbf{N}(i,j)} b\,d_k\left(C_l(i,j), C_l(g,h)\right), \quad (5)$$

where d_k is the Kronecker delta function and b is a constant that tunes the influence of spatial-contextual information on the change-detection process.

For the estimation of the class conditional energy functions $U_{data}(\cdot)$, we propose a novel adaptive semi-parametric technique based on the RPE [35] technique and the EM algorithm [34], [36]-[38]. In the next section, a detailed description of this technique is provided.

Finally, the minimization of (3) can performed by using different approaches (e.g. the *simulated annealing* algorithm [44]). In this paper, for the sake of simplicity, we shall adopt a simple and fast approach based on Besag's *iterated conditional modes* (ICM) algorithm [45].

The basic idea of the ICM algorithm consists in the relationship between the class labels for pixels, the current estimate of the labels of neighboring pixels, and the considered image (i.e., the difference image $\mathbf{X_D}$):

$$P\left(C_l(i,j)/X,\{C_l(g,h),(g,h)\in \mathbf{N}(i,j)\}\right) \propto P\left(X(i,j)/C_l(i,j)\right)P\left(C_l(i,j)/C_l(g,h)\right). \quad (6)$$

The implementation of the algorithm is as follows:

Step 1. Initialize $\mathbf{C}_l$ by assigning each pixel to the class that minimizes the non-contextual energy function $U_{data}(\cdot)$.

Step 2. For all pixels in the difference image, update the label with the one that minimizes equation (3).

Step 3. Repeat Step 2 until convergence is reached.

Convergence is reached when, at a given iteration, the number of pixels that modify the label is below a predefined threshold. It is worth noting that, even if the ICM algorithm converges to a local minimum of the energy function, it allows a good trade-off between computational complexity and accuracy obtained.

III. The Proposed Adaptive Semi-Parametric Estimation Technique

The estimation of the class conditional energy $U_{data}(X(i,j)/C_l(i,j))$ can be carried out under the pixel independence hypothesis, as the spatial-contextual information is assumed to be represented by the energy term $U_{context}(\cdot)$. Let us assume that the histogram $h_D(X)$ of the difference image $\mathbf{X_D}$ is an accurate estimate of its density function $p(X)$. We propose modeling $p(X)$ as a mixture density composed of the two components associated with the classes w_n and w_c, respectively, i.e.,

$$p(X) = p(X/w_n)P(w_n) + p(X/w_c)P(w_c). \quad (7)$$

The authors have already addressed the problem of estimating $p(X/w_n)$, $p(X/w_c)$, $P(w_n)$, and $P(w_c)$ in [34].

In that work, a parametric method was proposed that assumed Gaussian distributions for the class-conditional density functions $p(X/w_n)$ and $p(X/w_c)$. In this paper, we extend such an approach to the semi-parametric case by exploiting the RPE technique [35] and the EM algorithm [36]-[38]. A general scheme of the method is shown in Fig. 1. The method can be divided into two different phases:

1) initial non-parametric estimation of $p(X/w_n)$, $p(X/w_c)$, $P(w_n)$, and $P(w_c)$;

2) iterative semi-parametric optimization.

In the first phase (*non-parametric initialization*), a small number of pixels, which can be reasonably labeled as belonging to either w_n or w_c, are selected by exploiting the properties of the difference image together with the prior information that may be available for the specific problem considered. Then, on the basis of such pixels, the initial estimates of the statistical terms involved in (7) are derived with the non-parametric RPE technique. In the second phase (*iterative semi-parametric optimization*), the unlabeled pixels that are located in the middle region of the histogram, and that can turn out to be either changed or unchanged, are used to improve the estimates of the aforesaid statistical terms by performing an iterative process based on the EM algorithm. In the following, we describe these two phases in detail.

A. Non-parametric initialization

Let us assume that we can identify both a subset $\mathbf{S_n}$ of N_n pixels belonging to w_n and a subset $\mathbf{S_c}$ of N_c pixels belonging to w_c in the difference image $\mathbf{X_D}$. This is a reasonable assumption, if we consider the particular properties of the difference image: pixels with small gray-level values exhibit a high probability of being unchanged pixels, whereas pixels with large gray-level values are associated with a high probability of being changed pixels. In this context, we can define the initial sets of pixels $\mathbf{S_n}$ and $\mathbf{S_c}$ in terms of two thresholds, T_n and T_c, applied to the tails of the histogram $h_D(X)$ (i.e. $\mathbf{S_n} = \{X(i,j) | X(i,j) < T_n\}$ and $\mathbf{S_c} = \{X(i,j) | X(i,j) > T_c\}$), such that the subset $\mathbf{S_u} = \{X(i,j) | T_n \le X(i,j) \le T_c\}$ represents the pixels in the difference image $\mathbf{X_D}$ that cannot be easily identified as changed or unchanged pixels. Then both initial sets of pixels, $\mathbf{S_n}$ and $\mathbf{S_c}$, can be used to derive the initial estimates of the probability density functions $p(X/w_n)$ and $p(X/w_c)$ and of the prior probabilities of the classes $P(w_n)$ and $P(w_c)$.

Different strategies can be adopted in order to obtain two reasonable values of T_n and T_c, depending on the prior information available for the problem considered. Two simple strategies are described in the following.

The first strategy assumes that end-users rely on some prior information concerning the possible maximum and minimum extents of changed areas. In this case, T_n and T_c can be determined by fixing some constraints on the initial prior probabilities of the classes according to the information available. In particular, T_c can be selected as the threshold value that renders the cardinality of $\mathbf{S_c}$ equal to the number of pixels corresponding to the minimum extent of the changed area. A similar procedure can be adopted to select T_n.

The second strategy does not require any kind of prior information about the specific problem considered. It follows that, the initial thresholds can be selected by properly exploiting only the aforementioned peculiarities of the difference image. In particular, T_n and T_c can be defined in terms of the middle value M_D of the histogram $h_D(X)$ as:

$$T_n = M_D(1-a); \qquad T_c = M_D(1+a) \tag{8}$$

where a is a real number $(0 < a < 1)$ that defines the range around M_D in which pixels cannot be easily classified as either changed or unchanged pixels. M_D can be expressed by $M_D = (max\{\mathbf{X_D}\} - min\{\mathbf{X_D}\})/2$, where $max\{\mathbf{X_D}\}$ and $min\{\mathbf{X_D}\}$ are the maximum and minimum gray-level values in $\mathbf{X_D}$, respectively.

In both above-described cases, a precise selection of T_n and T_c is rather a difficult task. However, the objective of the initialization phase is not to obtain accurate estimates of the density functions and of the prior probabilities of the classes, but only a meaningful starting point for the next iterative estimation procedure.

Once T_n and T_c have been fixed, first rough estimates of $p(X/w_n)$, $p(X/w_c)$, $P(w_n)$ and $P(w_c)$ can be obtained from the initial sets of pixels, $\mathbf{S_n}$ and $\mathbf{S_c}$. On the one hand, the prior probabilities can be estimated by exploiting the relative frequencies of the pixels in the initial sets $\mathbf{S_n}$ and $\mathbf{S_c}$. On the other hand, the density functions of the classes can be estimated by using the nonparametric RPE technique (proposed by Fukunaga and Hayes in [35]), as described in the following.

The classical Parzen density estimate of $p(X/w_V)$ (with $w_v \in \{w_n, w_c\}$) is given by the following

equation:

$$\hat{p}_{N_v}(X/w_v) = \frac{1}{N_v} \sum_{X(i,j) \in S_v} \frac{1}{h} k\left[\frac{(X - X(i,j))}{h}\right], \tag{9}$$

where $k(\cdot)$ is a kernel function satisfying $\int k(X)dX = 1$, and h is the kernel-size control parameter. However, the use of the Parzen estimate may involve a very large number of kernel functions, which may render this estimation approach inappropriate to our purposes. In order to avoid this problem, according to [35], we propose to use a reduced number of representative kernels, selected so that the resulting estimates can be as close as possible to the Parzen estimate obtained with all available samples. In particular, when R_v representatives are selected from each set $\mathbf{S_n}$ (with $R_v << N_v$), the density function $p(X/w_V)$ is estimated by:

$$\hat{p}_{R_v}(X/w_v) = \frac{1}{R_v} \sum_{r=1}^{R_v} \frac{1}{h} k\left[\frac{(X - Y_r)}{h}\right], \tag{10}$$

where Y_r represents each of the R_v representative pixels. According to [35], the representative pixels R_v are selected from $\mathbf{S_n}$ so that the entropy between (10) and the corresponding true Parzen estimate (9) can be maximized [35]. In particular, the set of R_v representatives for the initial set of pixels $\mathbf{S_n}$ is computed by maximizing the following criterion function J_v:

$$J_v = \frac{1}{N_v} \sum_{X(i,j) \in S_v} \left\{ \mathbf{Ln}\left[\hat{p}_{R_v}(X(i,j)/\mathbf{w}_v)\right] - \mathbf{Ln}\left[\hat{p}_{N_v}(X(i,j)/\mathbf{w}_v)\right] \right\}. \tag{11}$$

The maximization of (11) is performed by the suboptimal search procedure proposed in [35]. The resulting estimates represent a reasonable starting point to derive the final density functions of changed and unchanged pixels in the difference image.

The selection of a model for the kernel functions is not a critical issue. However, taking into account the following iterative optimization phase carried out by the EM algorithm, we suggest the use of Gaussian-like functions. Concerning the selection of both the number of representatives and the initial smoothing parameter h, we followed the indications provided in [35]. However, it is worth noting that, in the present approach, the proposed iterative optimization step (see next paragraph) renders this selection less critical than in other cases, where, for instance, the smoothing parameter h is not optimized once it has been fixed.

According to Fukunaga and Hayes [35], the estimates obtained with the aforementioned approach can be considered non-parametric, as it does not require any a priory knowledge on the statistical models for the

distributions of changed and unchanged pixels in the difference image.

For a more detailed description of the RPE technique we refer the reader to [35].

B. Iterative semi-parametric optimization

The above-described initialization phase provides rather rough initial estimates of the required density functions as they are strongly biased by the two initial sets of pixels, $\mathbf{S_n}$ and $\mathbf{S_c}$. Therefore, it is necessary to improve such estimates by optimizing the set of parameters that characterize the corresponding density models. In this context, we propose to use the subset $\mathbf{S_u} = \mathbf{X_D} - \{\mathbf{S_n} \cup \mathbf{S_c}\}$ of pixels that cannot be easily classified as changed or unchanged pixels to increase iteratively the accuracies of the estimates of the statistical terms that define the mixture density *p(X)*. This procedure is carried out by applying the EM algorithm [36]-[38].

To accomplish such a task, a more flexible expression for the estimation of each density function $p(X/w_V)$ is proposed. In particular, the kernel-size control parameter may be different for each kernel; in addition, each kernel function is associated with a different weight such that the sum of the R_v weights associated with the class w_V may be equal to one. On the one hand, this increases the number of parameters to be estimated; on the other hand, it makes it possible to obtain more accurate approximations for the real distributions. It is worth noting that the aforementioned procedure implies the conversion of the non-parametric model (derived from the previous initialization phase) into a more suitable semi-parametric model. This semi-parametric model provides (by exploiting the unlabeled samples present in the subset $\mathbf{S_u}$) a more accurate description of the probability density functions of changed and unchanged pixels.

In this context, the new expression for each density function $p(X/w_V)$ can be obtained by rewriting expression (10) as:

$$\hat{p}_{R_v}(X/w_v) = \sum_{r=1}^{R_v} \frac{\Pi_{r,v}}{h_{r,v}} k\left[\frac{(X - Y_{r,v})}{h_{r,v}}\right]. \tag{12}$$

Using this formulation, the parameter vector to be optimized becomes $\boldsymbol{q}_v = \left[h_{1,v},...,h_{R_v,v},Y_{1,v},...,Y_{R_v,v},\Pi_{1,v},...,\Pi_{R_v,v}\right]$, where $h_{l,v}$, $Y_{l,v}$ and $\Pi_{l,v}$ represent the *l-th* kernel size control parameter, the *l-th* representative sample and the *l-th* weight, respectively, associated with the class

w_v.

The EM algorithm is initialized with the values derived from the initialization phase. Therefore, the initial parameters for the values of each class w_v are set to $h_{l,v}^0 = h$, $Y_{l,v}^0 = Y_{l,v}$ and $\Pi_{l,v}^0 = \frac{\hat{P}(w_v)}{R_v}$. It is possible to prove that, at each iteration of the EM algorithm, the estimated parameters provide an increase in the log-likelihood function $L(q) = \ln p(\mathbf{X_D} | q)$ (where $q = [q_n, q_c]$ is the parameter vector to be computed) [36]-[38]. At convergence, a local maximum of the log-likelihood function is reached. Although convergence can be ensured, it is not possible to guarantee that the algorithm will converge to the global maximum of the likelihood [36]-[38].

It is worth noting that, even if the EM algorithm usually requires a significant computational time, this aspect is not critical in our case, as we are dealing with a one-dimensional problem.

The estimates obtained at convergence (which is attained when the difference between the values of the log-likelihood function at two successive iterations is below a given threshold) can be used to derive the final estimate of the required energy function:

$$U_{data}(X(i,j), w_v) = -\mathbf{Ln}\left[p^{conv}(X / w_v)\right] = -\mathbf{Ln}\left[\sum_{r=1}^{R_v} \frac{P_{r,v}^{conv}}{h_{r,v}^{conv}} k\left(\frac{\left|X - Y_{r,v}^{conv}\right|}{h_{r,v}^{conv}}\right)\right]. \quad (13)$$

This expression can be used in (3) to generate the final change-detection map.

IV. Data Set Descriptions

In order to carry out an experimental analysis aimed at assessing the performances of the proposed approach, we considered two multitemporal data sets corresponding to geographical areas on the Peloponnesian Peninsula, Greece, and the Island of Elba, Italy, respectively. Detailed descriptions of such data sets are provided in the following.

A. Data Set Related to the Peloponnesian Peninsula

The first of the two data sets used in the experiments was composed of two images acquired in the same area by a passive multispectral scanner installed on a satellite (i.e. the Wide Field Sensor (WiFS) mounted on board the IRS-P3 satellite). The area shown in the two images was a section (512×512 pixels) of a scene

acquired in the southern part of the Peloponnesian Peninsula, Greece, in April 1998 and September 1998. As an example, Figs. 2(a) and (b) show channels 2 (i.e. near-infrared spectral channels) of both images. As is readily apparent, various wildfires destroyed a significant portion of the vegetation in the aforesaid area between the two dates. The available information concerning the locations of the wildfires was used to prepare a "reference map" (see in Fig. 2(c)) useful to assess change-detection errors. Such a map was refined by a manual analysis of the two remote-sensing images.

The images were registered by using the multispectral image acquired in April as a reference image. The analysis of the histograms of the April and September images did not reveal any significant difference in the light conditions at the two acquisition times. Therefore, no correction algorithms were required.

B. Data Set Related to the Island of Elba

The second data set used in the experiments was composed of a section (414×326 pixels) of two multispectral images acquired by the Thematic Mapper (TM) sensor installed on board of the Landsat-5 satellite. The two images were acquired in the western part of the Island of Elba, Italy, in August 1992 and September 1994. As an example, Figs. 3(a) and (b) show channels 4 (i.e. near-infrared spectral channels) of both images. As one can see by comparing the two images, a wildfire, which occurred in 1993, destroyed a significant part of the vegetation in the selected area. The damage is still evident in the September 1994 image. Also in this case, the available ground truth concerning the location of the wildfire was used to prepare a "reference map" (see Fig. 3(c)).

The images were registered by using the multispectral image acquired in 1992 as a reference image. In this case, too, no correction algorithms were applied as the analysis of the histograms of the two images did not reveal any significant difference in the light conditions at the two acquisition times.

V. EXPERIMENTAL RESULTS

A. Description of the Experiments

Four kinds of experiments were carried out to assess the effectiveness of the proposed technique on the two data sets considered. For the sake of simplicity, in all the trials made, we used the same values of the initial parameters of the classes of changed and unchanged pixels, i.e., $N_n = N_c = N$ and $h_n = h_c = h$.

First, the capabilities of the proposed adaptive semi-parametric technique for estimating the probability

density functions of changed and unchanged pixels were evaluated. To this end, the histograms of the considered difference images were normalized and compared with the estimates obtained by the proposed iterative estimation process.

Secondly, on the basis of the resulting estimates, both a qualitative and a quantitative analysis of the effectiveness of the presented technique were carried out. In particular, the change-detection map obtained by using the proposed technique was compared with the change-detection map provided by the application of the optimum decision threshold T_o that minimizes the overall change-detection error (i.e. the best result yielded by the classical thresholding method). To this end, the value of the optimum threshold T_o was achieved by applying a manual trial-and-error procedure to the difference image. This was accomplished by performing an accurate evaluation of the change-detection errors versus the values of the decision threshold and then by associating T_o with the value that gave the minimum overall change-detection error. This experiment aimed to demonstrate that the proposed technique is able to yield, in an automatic way, more accurate results than those obtainable by the classical non-automatic thresholding (CNT) approach.

In the third experiment, the accuracy provided by the proposed technique was compared with the accuracy exhibited by classical post-processing approaches used to reduce noise in the change-detection maps. In particular, the map provided by the proposed technique was compared with the change-detection map obtained by applying a classical filtering algorithm (a running median filter) to the minimum-error image derived by the CNT approach (i.e. by using the optimum decision threshold T_o). The objective of this experiment consists in assessing the effectiveness of the proposed spatial-contextual model to automatically provide accuracies higher than those that can be obtained by classical post-processing filtering approaches.

Finally, in the fourth experiment, the robustness of the proposed method versus the values of the main parameters selected in the initialization phase of the algorithm was assessed. To this end, the behavior of the overall change-detection error was evaluated by varying the values of α, N, h, and β. The results were compared with the minimum overall error resulting from the application of the CNT approach.

B. Results on the Data Set Related to the Peloponnesian Peninsula

In all the experiments, the difference image was computed by applying the *CVA* technique only to channels 2 of the multispectral images considered. This choice was made because such a spectral band was

found to be very effective in detecting burnt areas. In this experiment, no prior knowledge was assumed to be available for the initialization of the proposed technique; therefore, the performances of the proposed method were assessed under rather critical conditions.

For the first experiment, the initial thresholds, T_n and T_c, were selected by setting α equal to 0.5. As suggested in [35], the initial number N of kernels was fixed at 6 and the corresponding initial smoothing parameter h was set to 50. The result obtained is shown in Fig 4. As one can see, the obtained estimates of the density functions of the classes w_c and w_n provide an accurate description of the behavior of the histogram of the difference image. Such estimates were then used in equation (3) to derive the final change-detection map (the parameter β was set to 1.5). The resulting map of changes (see Fig. 5(a)) was compared both quantitatively and qualitatively with the change-detection map provided by the CNT approach (see Fig. 5(b)). The result of the quantitative comparison is shown in Table II. In particular, the table gives the numbers of false alarms (i.e. unchanged pixels identified as changed ones) and missed alarms (i.e. changed pixels categorized as unchanged ones) incurred by the proposed and classical approaches. As can be seen, the overall error obtained with the proposed technique (i.e. 2763 pixels) is smaller than the overall error resulting from the application of the manually determined threshold T_o (i.e. 3553 pixels). In greater detail, the number of missed alarms was reduced from 1129 to 1010 pixels, and the number of false alarms decreased from 2424 to 1753 pixels. This represents a significant improvement, considering that we have compared the proposed technique with the best result that can be obtained by the CNT. A better understanding of these results can be achieved by a qualitative analysis of the change-detection maps shown in Figs. 5(a) and (b). As one can see, the proposed technique provided, in an automatic way, a more accurate change-detection map than the one obtained by the application of the CNT approach. In particular, the use of the spatial-contextual information allowed a more precise identification of the changed areas and yielded a less noisy result.

At this point, the change-detection map provided by the proposed approach was compared with the maps derived by applying a running median filter to the minimum-error image yielded by the CNT approach. To this end, 3×3, 5×5, and 7×7 window sizes were used. In the best case (i.e. 3×3 window size), the overall error was reduced from 3553 pixels (provided by the pixel-by-pixel CNT approach) to 2973 pixels, whereas the error provided by the proposed automatic technique was smaller (i.e. 2763 pixels). This is a direct result of

the weak capabilities of filtering techniques to preserve borders of changed areas [46].

Finally, the robustness of the proposed technique to the initial values of the parameters involved in our approach was assessed. To this end, the change-detection map was obtained for different values of the parameters N, h, α and β. The resulting diagrams of the overall error versus the values of the different parameters are shown in Fig. 6. It is easy to see that the proposed technique presents rather a stable behavior. For instance, the overall errors obtained for different values of the parameter α (from 0.4 to 0.6) ranged from 1.00% (for $\alpha = 0.6$) to 1.05% (for $\alpha = 0.55$), 1.35% being the overall error provided by the CNT approach. The stablest behavior was observed for the parameter b, whereas the number N of kernels turned out to be the most critical parameter. However, it is worth noting that, in all the trials made, the overall error associated with the proposed method was always smaller than the error obtained by the CNT approach.

C. Results on the Data Set Related to the Island of Elba

For this data set, the difference image was computed by applying the *Change Vector Analysis* (CVA) method to images that had been filtered using a 3×3 mean filter. We applied the CVA technique to spectral bands 1, 2, 3, 5 and 7 of the two multispectral images, as preliminary experiments had demonstrated that this set of channels contains useful information for the detection of the damaged area.

In the first experiment, the initial parameters were fixed at α=0.5; N=6 and h=50, as for the previous data set. The results obtained are shown in Fig 7. As one can see, also in this case, the obtained estimates provide an accurate approximation for the histogram of the difference image. To evaluate the effectiveness of the proposed approach, the resulting estimates were used to derive the final change-detection map by minimizing equation (3) (the parameter β was set to 1.5) (see Fig. 8(a)). The overall error was quantitatively compared again with the one obtained by the CNT approach (see Table III). The proposed technique incurred an overall error (i.e. 1607 pixels) smaller than the one obtained with the CNT technique (i.e. 1936 pixels). In particular, the proposed method allowed decrements of both missed alarms (reduced from 1342 to 1326 pixels) and false alarms (reduced from 594 to 281 pixels). Also for this data set, the qualitative analyses of the two change-detection maps provided by the proposed technique (see Fig. 8(a)) and the CNT technique (see Fig. 8(b)) demonstrate the effectiveness of our method. In particular, the comparisons of the two maps with the reference image (see Fig. 3(c)) confirm the capability of the proposed method to provide, in an

automatic way, a change-detection map more reliable than the one resulting from the application of the CNT approach.

Also in this case, the change-detection map provided by the proposed approach was compared with the maps obtained by applying a running median filter (3×3, 5×5, and 7×7 window sizes were considered) to the minimum-error image yielded by the manual CNT approach. The results confirm the effectiveness of the proposed contextual approach. In particular, in the best case (i.e. 3×3 window size), the overall error was equal to 1707 pixels, whereas the proposed technique resulted in an overall error equal to 1607 pixels. As in the previous data set, the accuracy provided by the filtering approach decreases as the window size increases.

At this point, the robustness of the proposed technique to the initialization phase was evaluated. The results obtained are shown in Fig. 9. As one can see, the proposed technique exhibits a stable behavior versus the values of the initial parameters. For example, the overall errors associated with different values of α (i.e., from 0.4 to 0.6) ranged from 1.17% (for $\alpha = 0.6$) to 1.28% (for $\alpha = 0.4$), 1.43% being the overall error provided by the CNT. In greater detail, as for the previous data set, the stablest behavior was observed for the parameter b, whereas the least stable one was observed for the number N of kernels. However, in all the trials made, the proposed technique yielded better results than the CNT approach. This confirms the reliability and the effectiveness of the presented method.

VI. Conclusions

A novel automatic approach to unsupervised change detection in multitemporal remote-sensing images has been proposed. The presented approach is based on three theoretically well-founded methods for data and image analysis: the non-parametric RPE procedure [35], the EM algorithm [36]-[38] and MRFs [40]-[43]. The RPE technique is used to obtain rough non-parametric initial estimates of the density functions of the classes of changed and unchanged pixels in the difference image. Such estimates are iteratively improved by applying the EM algorithm in order to obtain a more accurate semi-parametric description of the statistics of the difference image. The resulting estimates are then used within the framework of an MRF approach to generate the change-detection map by taking into account also the spatial-contextual information contained in the difference image.

The proposed approach presents some important advantages over the classical unsupervised change-detection techniques that are typically used in remote-sensing applications: *i*) it provides a well-founded methodological framework for the automatic analysis of the difference image, thus avoiding heuristic approaches generally used in operational remote sensing; *ii*) it does not require any a-priori assumption for the statistical model of the distribution of changed and unchanged pixels in the difference image; *iii*) it allows the spatial-contextual information to be exploited efficiently in the change-detection process.

Experimental results reported in this paper point out the effectiveness of the proposed approach. In particular, in all the experiments carried out, the presented technique provided, in an automatic way, more accurate and less noisy change-detection maps than those obtained with the CNT technique. In addition, experiments highlighted the stability of the presented approach versus the values of the initial parameters. However, even though in all our experiments we always obtained a good stability, we think that the most critical step in the initialization phase of the algorithm lies in deriving the two initial sets of pixels, $\mathbf{S}_n$ and $\mathbf{S}_c$. Therefore, if possible, we suggest using any kind of prior knowledge available concerning the specific problem faced (e.g. expected maximum and minimum extents of changed areas, shapes or spatial distributions of changes) in order to derive these subsets in the most accurate possible way. This may result in a more precise change-detection map.

An important characteristic of the proposed approach is that it does not assume any a priori model for the density functions of changed and unchanged pixels in the difference image. Consequently, it can be applied to different types of images (e.g. SAR images [47], optical images, etc.).

In terms of computation time, the proposed method is quite fast. In fact, the phase of the estimation of the statistical terms of changed and unchanged pixels, which is the most time-consuming phase of the algorithm, requires a low computational load, thanks to the fact that the estimation process is carried out in a one-dimensional space.

It is worth noting that the change-detection map resulting from the application of the MRF approach might be used to derive more accurate estimates of the density functions of the classes. In this context, these estimates might be used again in (3) to derive a new change-detection map. Such a process might be iterated in order to increase the accuracy of the final change-detection result. However, the slight improvement in the final result obtainable by this approach may not justify the considerable increase in the computation time required.

Two limits of the proposed approach may be associated with a possible very low frequency of changed pixels or with a low contrast in the difference image. However, in operational remote-sensing applications, these problems can be addressed in advance by selecting a suitable space-borne sensor. On the one hand, a sufficient spatial resolution may allow the changed area to be identified with the required spatial scale, thus minimizing the problem of a "too small" prior probability for the changed pixels. On the other hand, suitable spectral bands or a suitable set of features derived from the original images (e.g., texture features) may allow the land-cover changes of interest (e.g., forest to burned area, grassland to flooded area) to be clearly pointed out in the difference image, thus reducing the potential problem of low contrast.

As a final remark, it is important to note that, although the proposed method has been presented in the specific context of the analysis of multitemporal remote-sensing images, it exhibits general characteristics, hence it could be used in any change-detection application requiring a technique based on the difference image.

ACKNOWLEDGMENTS

This research was supported by the Italian Space Agency (ASI). The authors wish to thank the Space Applications Institute (SAI) of the Joint Research Center (JRC) for providing the multitemporal images of the Peloponnesian Peninsula. They are also grateful to the anonymous reviewers for their constructive criticism.

REFERENCES

[1] M. J. Carlotto, "Detection and analysis of change in remotely sensed imagery with application to wide area surveillance," *IEEE Trans. on Image Processing*, vol. 6, no. 1, pp. 189-202, 1997.

[2] *Proc. of the IEEE Workshop on Visual Surveillance*, Bombay, India, January 1998.

[3] D. Le Gall, "MPEG: A video compression standard for multimedia applications," *Communications of the ACM*, vol. 34, no. 4, pp. 47-58, 1991.

[4] S. G. Mallat, "A theory for multiresolution signal decomposition: the wavelet representation," *IEEE Trans. on Pattern Analysis and Machine Intelligence*, vol. 11, no. 7, pp. 674-692, 1989.

[5] L. H. Chen and S. Chang, "A video tracking system with adaptive predictors," *Pattern Recognition*, vol. 25, no. 10, pp. 1171-1180, 1992.

[6] W. Y. Kan, J. V. Krogmeier, and P.C. Doerschuk, "Model-based vehicle tracking from image sequences with an application to road surveillance," *Optical Engineering*, vol. 35, no. 6, pp. 1723-1729, 1996.

[7] S. C. Liu, C. W. Fu, and S. Chang, "Statistical change detection with moments under time-varying illumination," *IEEE Trans. on Image Processing*, vol. 7, no. 9, pp. 1258-1268, 1998.

[8] C. W. Fu and S. Chang, "A motion estimation algorithm under time-varying illumination case," *Pattern Recognition Letters*, vol. 10, no. 3, pp. 195-199, 1989.

[9] L. Bruzzone and S. B. Serpico, "An iterative technique for the detection of land-cover transitions in multitemporal remote-sensing images," *IEEE Trans. on Geoscience and Remote Sensing*, vol. 35, no. 4, pp. 858-867, 1997.

[10] J. R. G. Townshend, C. O. Justice, and C. Gurney, "The impact of misregistration on change detection," *IEEE Trans. on Geoscience and Remote Sensing*, vol. 30, no. 5, pp. 1054-1060, 1992.

[11] L. Bruzzone and S. B. Serpico, "Detection of changes in remotely sensed images by the selective use of multi-spectral information," *Int. Journal of Remote Sensing*, vol. 18, no. 18, pp. 3883-3888, 1997.

[12] T. Fung, "An assessment of TM imagery for land-cover change detection," *IEEE Trans. on Geoscience and Remote Sensing*, vol. 28, no. 12, pp. 681-684, 1990.

[13] A. Singh, "Digital change detection techniques using remotely sensed data," *Int. Journal of Remote Sensing*, vol. 10, no. 6, pp. 989-1003, 1989.

[14] J. R. G. Townshend and C. O. Justice, "Spatial variability of images and the monitoring of changes in the normalized difference vegetation index," *Int. Journal of Remote Sensing*, vol. 16, no. 12, pp. 2187-2195, 1995.

[15] D. Wiemker, "An iterative spectral-spatial bayesian labeling approach for unsupervised robust change detection on remotely sensed multispectral imagery," *Proc. of the 7th International Conference on Computer Analysis of Images and Patterns, G. Sommer, K. Daniilidis and J. Pauli (Ed.), Lecture Notes in Computer Science, Springer Verlag, Heidelberg*, vol. 1296, pp. 263-270, 1997.

[16] A. A. Nielsen, K. Conradsen, J. J. Simpson, "Multivariate alteration detection (MAD) and MAF processing in multispectral, bitemporal image data: new approaches to change detection studies," *Remote Sensing of Environment*, vol. 64, no. 1, pp. 1-19, 1998.

[17] J. Flusser and T. Suk, "A moment-based approach to registration of images with affine geometric distortion," *IEEE Trans. on Geoscience and Remote Sensing*, vol. 32, no. 2, pp. 382-387, 1994.

[18] D. I. Barnea and H. F. Silverman, "A class of algorithms for fast digital image registration," *IEEE Trans. on Computers*, vol. C-21, no. 2, pp. 179-186, 1972.

[19] J. Ton and A. K. Jain, "Registering Landsat images by point matching," *IEEE Trans. on Geoscience and Remote Sensing*, vol. 27, no. 5, pp. 642-650, 1989.

[20] T. F. Knoll and E. J. Delp, "Adaptive gray scale mapping to reduce registration noise in difference images," *Computer Vision, Graphics, and Image Processing*, vol. 33, pp. 129-137, 1986,

[21] P. Gong, E. F., Ledrew and J. R. Miller, "Registration-noise reduction in difference images for change detection," *Int. Journal of Remote Sensing*, vol. 13, no. 4, pp. 773-779, 1992.

[22] P. S. Chavez, Jr., "Radiometric calibration of Landsat Thematic Mapper multispectral images," *Photogrammetric Engineering & Remote Sensing*, vol. 55, no. 9, pp. 1285-1294, 1989.

[23] P. S. Chavez, Jr. and D. J. MacKinnon, "Automatic detection of vegetation changes in the

southwestern United States using remotely sensed images," *Photogrammetric Engineering & Remote Sensing*, vol. 60, no. 5, pp. 1285-1294, 1994.

[24] J. A. Richards, *Remote Sensing Digital Image Analysis*, 2nd ed., New York: Springer-Verlag, 1993.

[25] P. N. Slater, "Reflectance and radiance based methods for the in-flight absolute calibration of multispectral sensors," *Remote Sensing of Environment,* vol. 22, pp.11-37, 1987.

[26] P. M. Teillet, P. N. Slater, Y. Ding, R. P. Santer, R. D. Jackson, and M. S. Moran, "Three methods for the absolute calibration of the NOAA AVHRR sensors in flight," *Remote Sensing of Environment*, vol. 31, pp.105-120, 1990.

[27] H. Olsson, "Reflectance calibration of thematic mapper for forest change detection," *Int. Journal of*

[28] P. L. Rosin, "Unimodal thresholding", *Patter Recognition,* (in press).

[29] T. Fung and E. LeDrew, "The determination of optimal threshold levels for change detection using various accuracy indices," *Photogrammetric Engineering & Remote Sensing*, vol. 54, no. 10, pp. 1449-1454, 1988.

[30] K. Fukunaga, *Introduction to Statistical Pattern Recognition*, 2nd ed., London: Academic Press, 1990.

[31] M. L. Stauffer and R. L. McKinney, *Landsat image differencing as an automated land cover change detection technique*, Technical Memorandum Rep. CSC/TM-78/6215, Computer Science Corporation, Silver Springs, Maryland, USA, 1978.

[32] R. F. Nelson, "Detecting forest canopy change due to insect activity using Landsat MSS," *Photogrammetric Engineering & Remote Sensing*, vol. 49, pp. 1303-1314, 1983.

[33] A. Singh, *Tropical forest monitoring using digital Landsat data in northeastern India*, Ph.D. thesis, University of Reading, Reading, England, 1984.

[34] L. Bruzzone and D. Fernàndez Prieto, "Automatic analysis of the difference image for unsupervised change detection," *IEEE Trans. on Geoscience and Remote Sensing*, vol. 38, no. 3, pp. 1171-1182, 2000.

[35] K. Fukunaga and R. Hayes, "The reduced Parzen classifier," *IEEE Transactions on Pattern Analysis and Machine Intelligence*, vol. 11, no. 4, 1989.

[36] A. P. Dempster, N. M. Laird, and D. B. Rubin, "Maximum likelihood from incomplete data via the EM algorithm," *Journal of Royal Statistic. Soc.*, vol. 39, no. 1, pp. 1-38, 1977.

[37] T.K. Moon, "The Expectation-Maximization algorithm," *Signal Processing Magazine*, vol.13, no.6, pp. 47-60, 1996.

[38] A. P. Redner and H. F. Walker, "Mixture densities, maximum likelihood and the EM algorithm," *SIAM Review*, vol. 26, no. 2, pp.195-239, 1984.

[39] D. A. Landgrebe, "The development of a spectral-spatial classifier for earth observational data," *Pattern Recognition*, vol. 12, pp. 165-175, 1980.

[40] R. Chellapa and A. Jain, Eds., *Markov Random Fields: Theory and Applications*. New York: Academic, 1993.

[41] R. C. Dubes and A. K. Jain, "Random field models in image analysis," *J. Appl. Statist.*, vol. 16, pp. 131-163, 1989.

[42] E. Rignot and R. Chellappa, "Segmentation of polarimetric synthetic aperture radar data," *IEEE Transactions on Image Processing*., vol. 1, no. 3, pp. 281-300, 1992.

[43] A. H. Schistad Solberg, A. K. Jain, and T. Taxt, "Fusion of multitemporal satellite images and GIS data for land-use classification," *IEEE Transactions in Geoscience and Remote Sensing*, vol. 32, no. 4, pp. 768-778, 1994.

[44] S. Geman and D. Geman, "Stochastic relaxation, Gibbs distributions, and the Bayesian restoration of images," *IEEE Transactions on Pattern Analysis and Machine Intelligence*, vol. PAMI-6, no. 6, pp. 721-741, 1984.

[45] J. Besag, "On the statistical analysis of dirty pictures," *J. Royal Statist. Soc.*, ser. B, vol. 48, pp. 259-302, 1986.

[46] L. Bruzzone and D. Fernàndez Prieto, "An adaptive parcel-based technique for unsupervised change detection," *International Journal of Remote Sensing*, Vol. 21, No. 4, 2000.

[47] L. Bruzzone and D. Fernandez Prieto, "Unsupervised change detection in multisource and multisensor remote sensing images," *Proc. of the IEEE 2000 Int. Geoscience and Remote Sensing Symposium (IGARSS 2000)*, Honolulu, Vol. VI, pp. 2441-2443, July 2000.

FIGURE CAPTIONS

Fig. 1. Schematic representation of the proposed adaptive semi-parametric estimation technique.

Fig. 2. Images of the Peloponnesian Peninsula, Greece, utilized in the experiments: (a) NIR band of the IRS-PE WiFS image acquired in April 1998; (b) NIR band of the IRS-PE WiFS image acquired in September 1998; (c) ground-truth map of the changed area used as a reference map in the experiments.

Fig. 3. Images of the Island of Elba, Italy, utilized in the experiments: (a) band 4 of the Landsat TM image acquired in August 1994; (b) band 4 of the Landsat TM image acquired in September 1994; (c) ground-truth map of the changed area used as a reference map in the experiments.

Fig. 4. Histogram of the difference image corresponding to the data set related to the Peloponnesian peninsula. For the sake of comparison, the estimates obtained by the proposed technique for the densities of the two classes, w_n and w_c, are superimposed. The histogram has been normalized in order to permit a direct comparison with the estimated distributions of the classes.

Fig. 5. Change-detection maps obtained for the images related to the Peloponnesian Peninsula: (a) proposed technique; (b) CNT technique.

Fig. 6. Behaviors of the change-detection error (%) versus the values of the initial set of parameters used for the images related to the Peloponnesian Peninsula: (a) α; (b) N; (c) h; (d) b.

Fig. 7. Histogram of the difference image corresponding to the data set related to the Island of Elba. For the sake of comparison, the estimates obtained by the proposed technique for the densities of the two

classes, w_n and w_c, are superimposed. The histogram has been normalized in order to permit a direct comparison with the estimated distributions of the classes.

Fig. 8. Change-detection maps obtained for the images related to the Island of Elba: (a) proposed technique; (b) CNT technique.

Fig. 9. Behaviors of the change-detection error (%) versus the values of the initial set of parameters used for the images related to the Island of Elba: (a) α; (b) N; (c) h; (d) b.

TABLE CAPTIONS

TABLE I. Legend of notations used in this paper.

TABLE II. Overall error, false and missed alarms resulting from the application of the proposed technique to the data set related to the Peloponnesian peninsula. For the sake of comparison, the table also gives the overall error, false and missed alarms involved by the CNT technique.

TABLE III. Overall error, false and missed alarms resulting from the application of the proposed technique to the data set related to the Island of Elba. For the sake of comparison, the table also gives the overall error, false and missed alarms involved by the CNT technique.

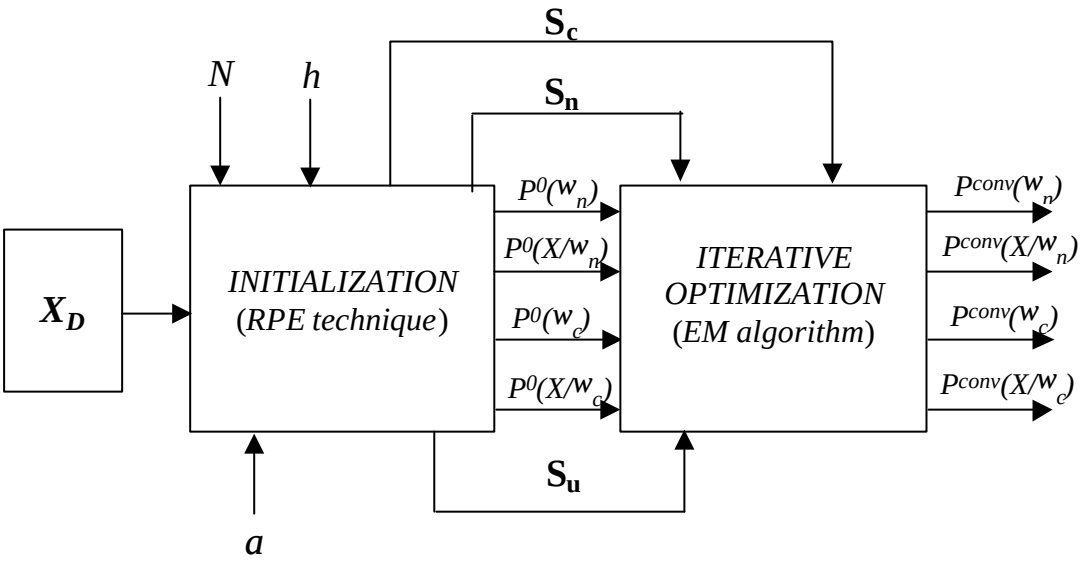
S_c
N
h
S_n
P^0(w_n)
P^0(X/w_n)
P^0(w_c)
P^0(X/w_c)
P^conv(w_n)
P^conv(X/w_n)
P^conv(w_c)
P^conv(X/w_c)
X_D
INITIALIZATION
(RPE technique)
ITERATIVE
OPTIMIZATION
(EM algorithm)
S_u
a

Fig. 1

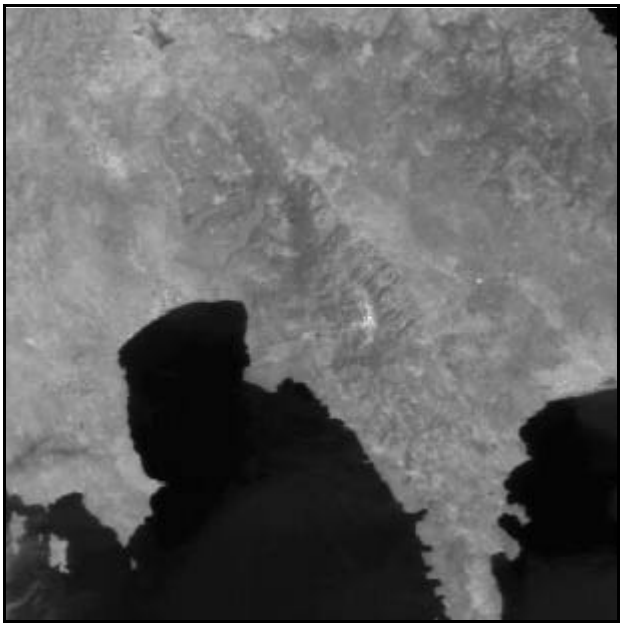

(a)

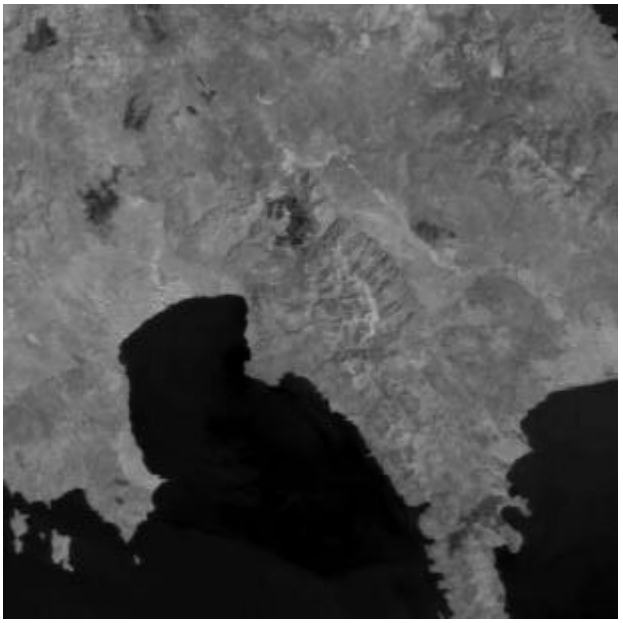

(b)

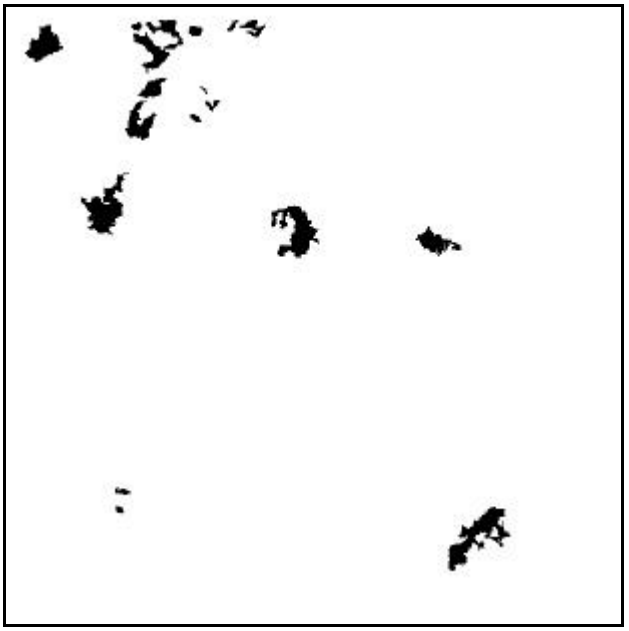

(c)

Fig. 2

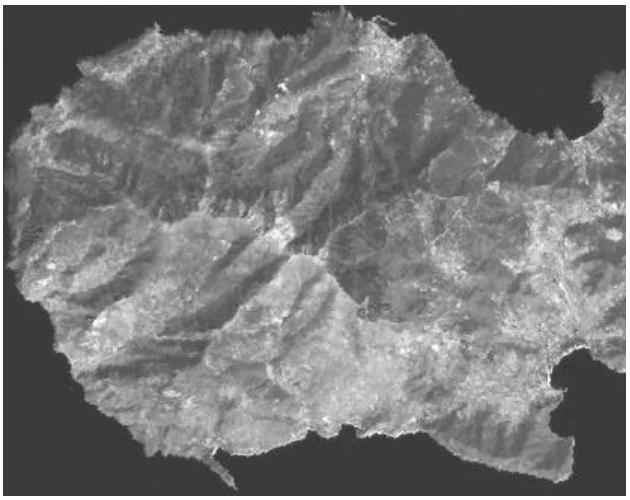

(a)

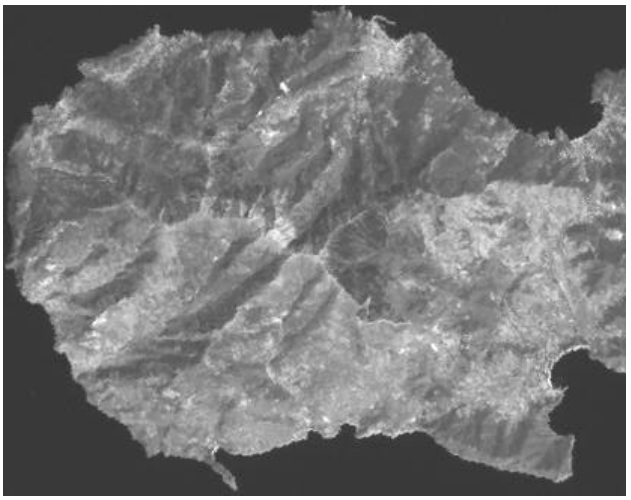

(b)

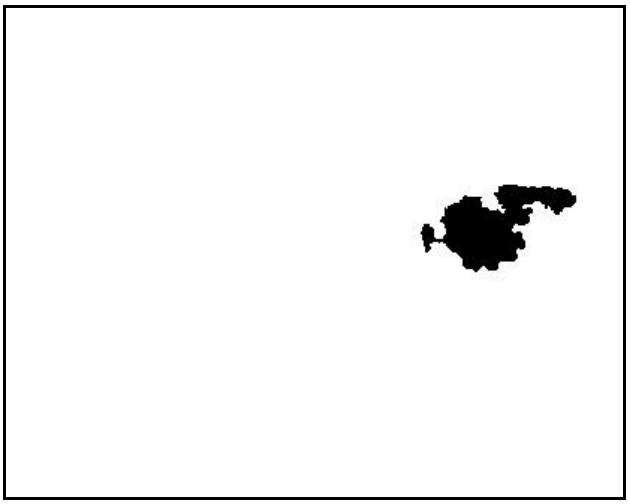

(c)

Fig. 3

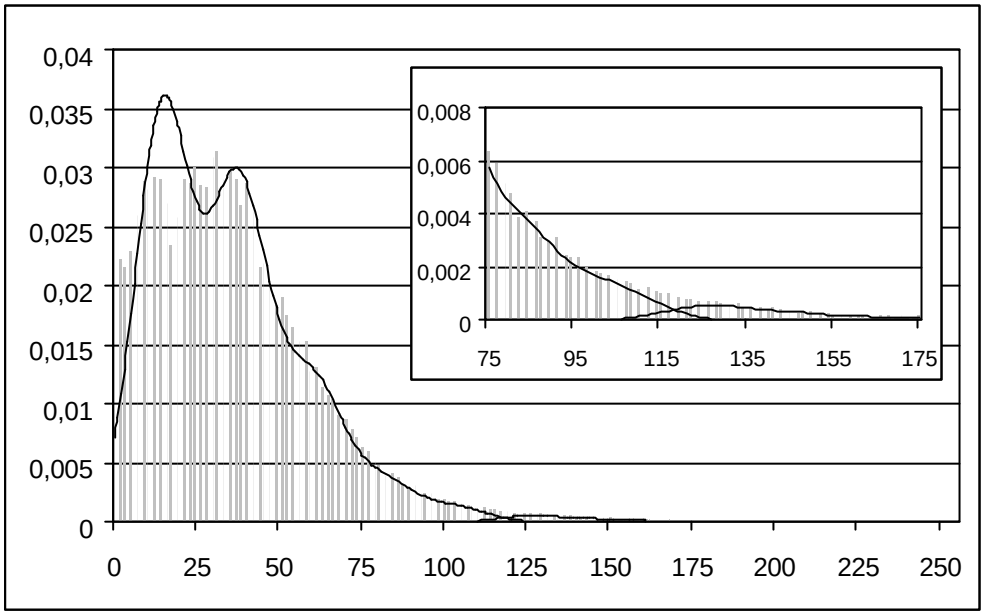
0,04
0,035
0,03
0,025
0,02
0,015
0,01
0,005
0
0
25
50
75
100
125
150
175
200
225
250
0,008
0,006
0,004
0,002
0
75
95
115
135
155
175

Fig. 4

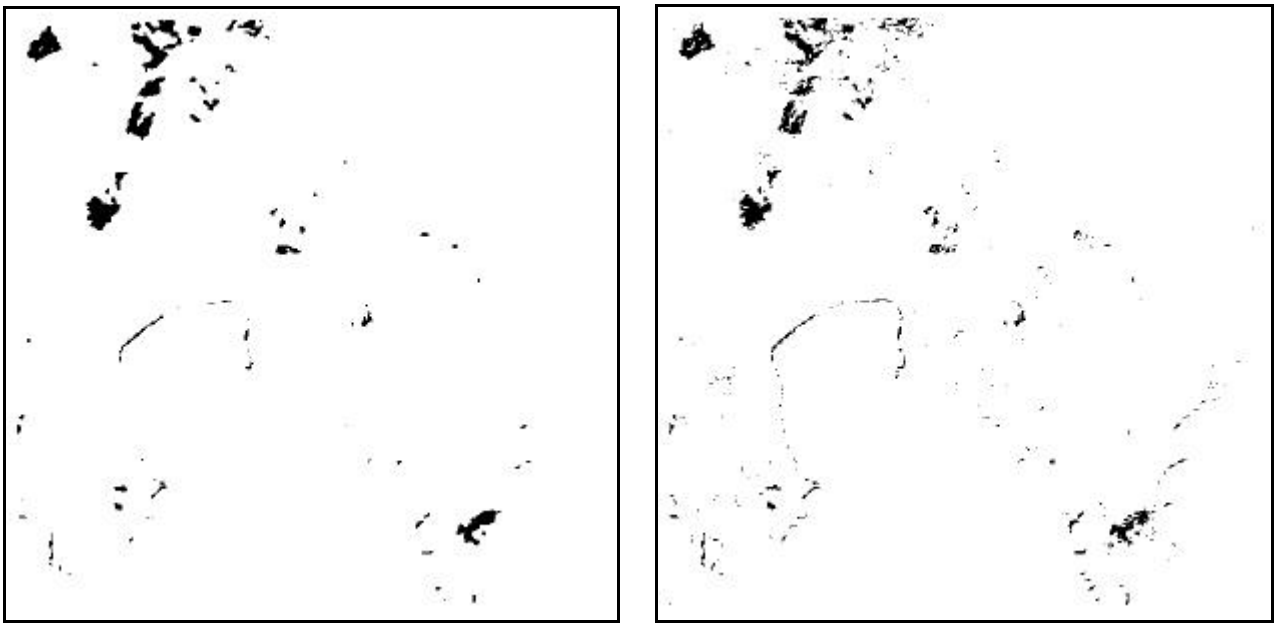

(a) (b)

Fig. 5

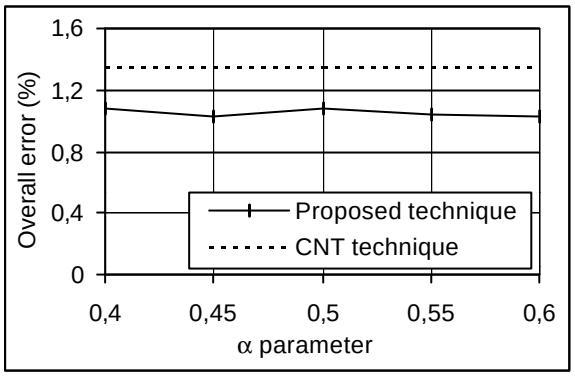
1,6
1,2
0,8
0,4
0
Overall error (%)
Proposed technique
CNT technique
0,4
0,45
0,5
0,55
0,6
α parameter

(a)

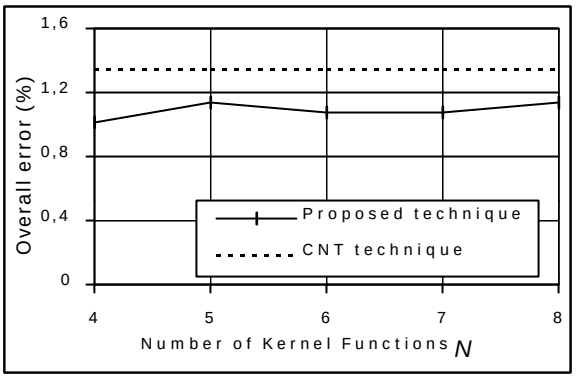
1,6
1,2
0,8
0,4
0
Overall error (%)
Proposed technique
CNT technique
4
5
6
7
8
Number of Kernel Functions N

(b)

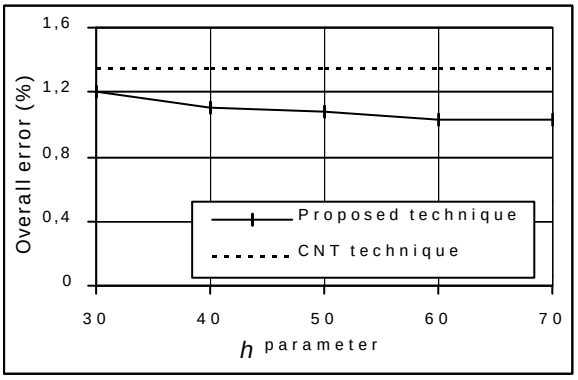
1,6
1,2
0,8
0,4
0
Overall error (%)
Proposed technique
CNT technique
30
40
50
60
70
h parameter

(c)

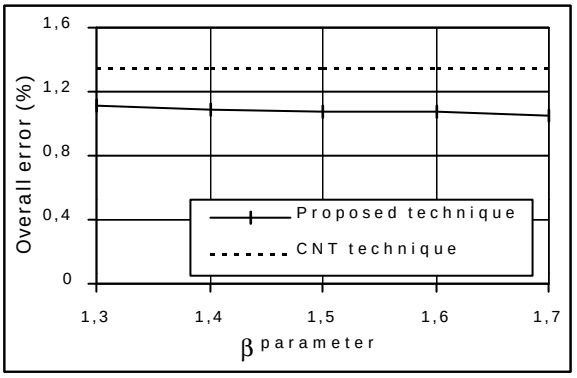
1,6
1,2
0,8
0,4
0
Overall error (%)
Proposed technique
CNT technique
1,3
1,4
1,5
1,6
1,7
β parameter

(d)

Fig. 6

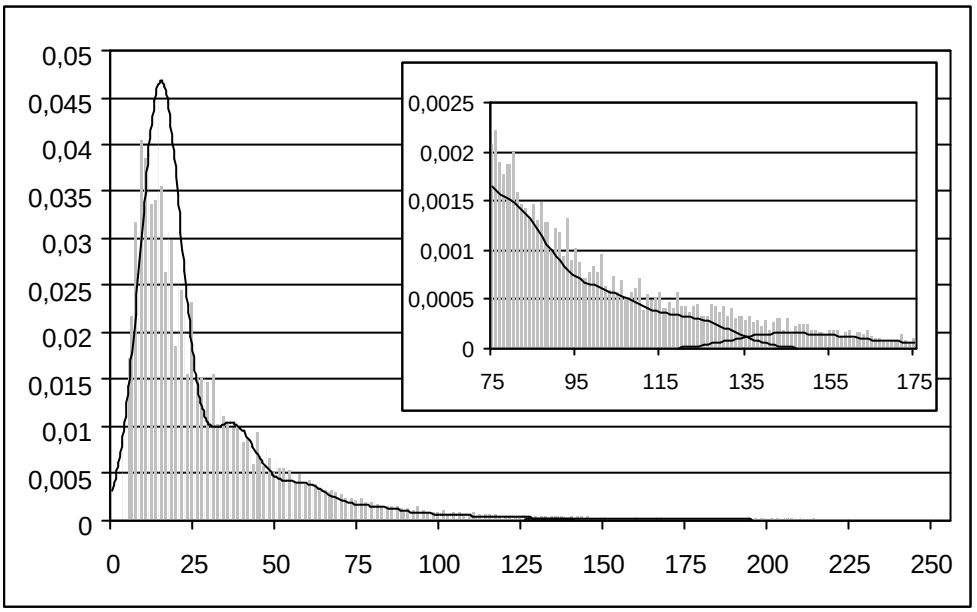
0,05
0,045
0,04
0,035
0,03
0,025
0,02
0,015
0,01
0,005
0
0
25
50
75
100
125
150
175
200
225
250
0,0025
0,002
0,0015
0,001
0,0005
0
75
95
115
135
155
175

Fig. 7

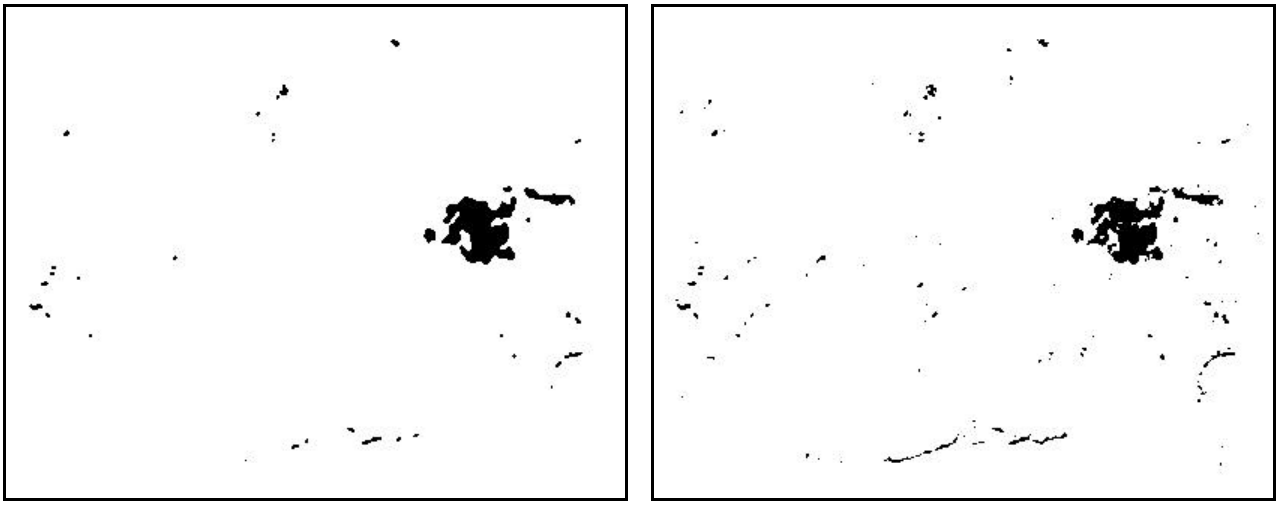

(a) (b)

Fig. 8

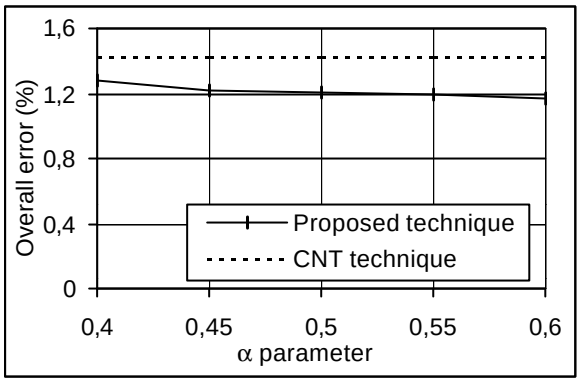
1,6
1,2
0,8
0,4
0
Overall error (%)
Proposed technique
CNT technique
0,4
0,45
0,5
0,55
0,6
α parameter

(a)

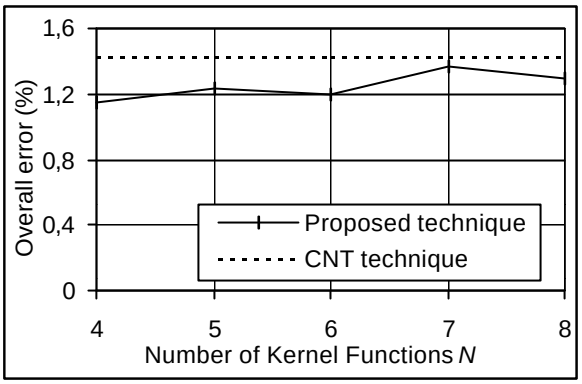
1,6
1,2
0,8
0,4
0
Overall error (%)
Proposed technique
CNT technique
4
5
6
7
8
Number of Kernel Functions N

(b)

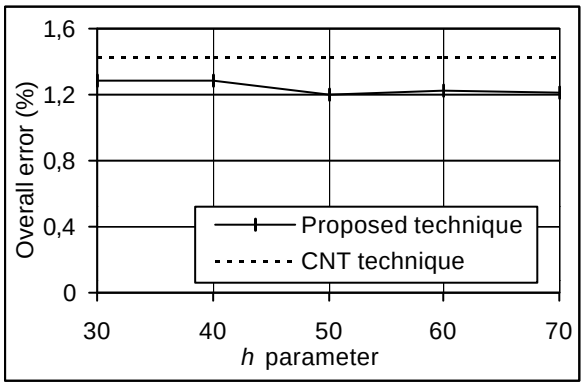
1,6
1,2
0,8
0,4
0
Overall error (%)
Proposed technique
CNT technique
30
40
50
60
70
h parameter

(c)

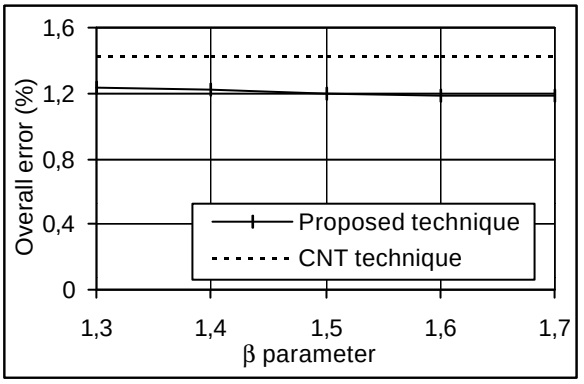
1,6
1,2
0,8
0,4
0
Overall error (%)
Proposed technique
CNT technique
1,3
1,4
1,5
1,6
1,7
β parameter

(d)

Fig. 9

TABLE I

Symbol	Description
$\mathbf{X_i}$	Image acquired at the time t_i
$\mathbf{X_i^{AOI}}$	Area of interest, extracted from image $\mathbf{X_i}$
I, J	Dimensions of the selected area of interest
$X_i^{AOI}(i, j)$	Feature vector of coordinates (i,j) belonging to $\mathbf{X_i^{AOI}}$
$\mathbf{X_D}$	Difference image
X	Random variable that represents the pixel values in $\mathbf{X_D}$
$X(i, j)$	Value of pixel of coordinates (i,j) belonging to $\mathbf{X_D}$
ω_c, ω_n	Classes associated with changed and unchanged pixels, respectively
$\boldsymbol{C}$	Set of all possible sets of labels in $\mathbf{X_D}$
$\boldsymbol{C}_l$	Generic set of labels in $\mathbf{X_D}$
$\boldsymbol{N}(i,j)$	Neighbor system of the pixel with the coordinates (i,j)
$h_D(X)$	Histogram of $\mathbf{X_D}$
M_D	Middle value of the histogram $h_D(X)$
$\mathbf{S_n}, \mathbf{S_c}, \mathbf{S_u}$	Sets of pixels used for initializing the proposed technique
α	Initialization parameter
T_n , T_c	Initial threshold values used for defining $\mathbf{S_n}$, $\mathbf{S_c}$, and $\mathbf{S_u}$
$U(\cdot)$	Energy functions
$k(\cdot), h$	Kernel function and corresponding smoothing parameter
$h_{i,j}, Y_{i,j}, \Pi_{i,j}$	Parameters that describe the class-conditional energy function $U_{data}(\cdot)$
N_j, R_j	Cardinality of $\mathbf{S_j}$ and number of selected representatives, respectively
β	Parameter that tunes the influence of spatial-contextual information
δ_k	Kronecker delta function
T_o	Minimum-error threshold

TABLE II

Approach	False alarms	Missed alarms	Overall error
Proposed	1010	1753	2763
CNT	1129	2424	3553

TABLE III

Approach	False alarms	Missed alarms	Overall error
Proposed	281	1326	1607
CNT	594	1342	1936